Assessment of Pole Erosion in a Magnetically Shielded Hall Thruster

Ioannis G. Mikellides* and Alejandro L. Ortega,†
Jet Propulsion Laboratory, California Institute of Technology, Pasadena, CA, 91109

Abstract: Numerical simulations of a 6-kW laboratory Hall thruster called H6 have been performed to quantify the erosion rate at the inner pole. The assessments have been made in two versions of the thruster, namely the unshielded (H6US) and magnetically shielded (H6MS) configurations. The simulations have been performed with the 2-D axisymmetric code Hall2De which employs a new multi-fluid ion algorithm to capture the presence of low-energy ions in the vicinity of the poles. It is found that the maximum computed erosion rate at the inner pole of the H6MS exceeds the measured rate of back-sputtered deposits by ~4.5 times. This explains only part of the surface roughening that was observed after a 150-h wear test, which covered most of the pole area exposed to the plasma. For the majority of the pole surface the computed erosion rates are found to be below the back-sputter rate and comparable to those in the H6US which exhibited little to no sputtering in previous tests. Possible explanations for the discrepancy are discussed.

Since their inception over several decades ago the application of Hall thrusters has been constrained to near-Earth missions largely due to their limited throughput capability. The source of this limitation has been erosion of the acceleration channel walls, which can lead to exposure of critical magnetic circuit components to the high-energy ion beam and, eventually, to engine failure. A new technique has been demonstrated to eliminate channel erosion in Hall thrusters [1-3] based on findings from physics-based numerical simulations with a magnetic-field-aligned-mesh (MFAM) code called *Hall2De* [4] and results from a Qualification Life Test (QLT) of the BPT-4000.[5] The BPT-4000 is a commercial Hall thruster designed and built by Aerojet-Rocketdyne that reached a zero-erosion state upon conclusion of the QLT.[6] Termed "magnetic shielding" [5] the technique enforces the equipotentialization of specific magnetic field lines called "grazing lines" which, in turn, protect the channel walls from ion bombardment. The demonstration of the first principles of magnetic shielding took place at the Jet Propulsion Laboratory (JPL) in 2010-2012. During this 2-yr, proof-of-principle effort a 6-kW laboratory Hall thruster called H6 [7], was modified from its original configuration - called hereinafter the unshielded configuration or H6US – based on the guidance of numerical simulations with the Hall2De code. The magnetically shielded configuration, or H6MS, was then wear tested for 150 h at 300 V, 6 kW (20 A) and the erosion rates of the acceleration channel were found to be 2-3 orders of magnitude lower than those in the H6US. These measured rates were in agreement with the numerical simulation predictions. More recently, numerical simulations of the H6MS were performed for the discharge voltage range of 400-700 V at constant power (6 kW) and at 800 V, 9 kW.[8] The simulations were followed by performance and wear testing at the 800 V, 9 kW operating condition.[9] The combination of simulations and tests showed that the effectiveness of magnetic shielding to reduce channel erosion by at least a few orders of magnitude was retained at higher discharge voltages so long as the magnetic circuit was capable of supplying the intended magnetic field topology.[8]

The findings on the effectiveness of magnetic shielding at discharge voltages >300 V is of immediate significance to ongoing thruster development and testing activities at the NASA Glenn Research Center (GRC) and JPL aimed at supporting NASA's Asteroid Initiative, which includes a proposal to robotically capture a small near-Earth asteroid and redirect it safely to a stable orbit in the Earth-moon system where astronauts can visit and explore it (Fig. 1).[10]

* Principal Engineer, Electric Propulsion Group, 4800 Oak Grove Drive, Pasadena, CA, 91109, Mail Stop 125-109, Associate Fellow AIAA.
† Member of the Technical Staff, Electric Propulsion Group, 4800 Oak Grove Drive, Pasadena, CA, 91109, Mail Stop 125-109, Associate Fellow AIAA.

Trajectory studies have shown that an Asteroid Redirect Mission (ARM) will require Hall thrusters operating at a specific impulse (I_{sp}) of ~3000 s. (~800 V) [11, 12]. Moreover, these thrusters will be expected to deliver a throughput of 12,000 kg of xenon [12], which is nearly a factor 30 greater than the 425 kg launched on the Dawn mission (the largest xenon propellant load launched to date). In response, NASA's Space Technology Mission Directorate, In Space Propulsion Project is supporting investigations of magnetic shielding in high-I_{sp} thrusters. These investigations include numerical simulations, thruster modifications and testing of the NASA 300M [13] - a 20-kW Hall thruster developed at GRC - and of the H6MS Hall thruster developed at JPL [14-16].

Fig 1. The Asteroid Redirect Mission (ARM) proposes to capture robotically a small near-Earth asteroid and redirect it safely to a stable orbit in the Earth-moon system. ARM will require long-life Hall thrusters that can deliver 3000 sec of I_{sp} (input voltage to each thruster of ~800 V).

While no evidence of channel erosion was observed during the original 2-yr effort at 300 V, 6 kW the inner pole surface appeared grated after the 150-h wear test. Some roughening also appeared along a thin strip surrounding the exposed surface of the outer pole. Figure 2 shows photographs of the H6MS before (left) and after (right) the 150-h wear test at 300 V, 6 kW. Evident is the darkening of the insulator rings (originally of white color) caused by carbon deposition from the test facility. Also evident is the roughening of the poles suggesting that some sputtering may had occurred.

The objective of the work reported in this paper is to explain, quantify and mitigate, if necessary, any sputtering of the poles due to ion bombardment. Section I provides a brief background on the first principles of magnetic shielding in Sec. I.A followed by a description of the computational model in Sec. I.B that was used to perform the plasma simulations. Section I.C. outlines a wide range of comparisons between simulation results and measurements in both the H6US and H6MS versions of the thruster. The erosion model and results are presented in Sec. II. Section III discusses the results and provides possible explanations for the observed texture of the poles. Concluding remarks are provided in Section IV.

Fig 2. Left: The H6MS before wear testing. The acceleration channel rings appear white and no surface roughening of the inner pole surface is evident. Right: The H6MS after a 150-h wear test in a JPL facility at 300 V and 20 A. The channel rings appear dark as the reduced erosion rates fell well below the deposition rates, allowing for build-up of carbon onto the ring surfaces. Roughening of the inner and outer pole surfaces became evident suggesting some sputtering could have occurred.

I. Numerical Simulations of the H6US and H6MS Thruster Configurations

A. Magnetic Shielding First Principles

The theory behind magnetic shielding was discussed in detail in previous publications. [1-3] In this section we provide only a summary of the main points for completeness. Under typical discharge conditions in Hall thrusters the resistance to the transport of heat and mass in the electron flow in a direction parallel (‖) to the magnetic field **B** is much smaller (by $\sim\Omega_e^2$ where Ω_e is the Hall parameter) than that in the ⊥ direction for most of the channel region. Thus, the electron temperature T_e remains relatively unchanged along the lines of force:

$$\nabla_{\parallel} T_e \approx 0 . \tag{1}$$

Moreover, in the absence of a resistive contribution to the electric field **E** in this direction the electron momentum equation simplifies to:

$$\mathbf{E}_{\parallel} \approx -T_e \nabla_{\parallel} \ell n(n_e) \tag{2}$$

where n_e is the electron number density. Equations (1) and (2) yield respectively two well-known properties of the lines of force in these thrusters [17, 18]: $T_e \approx T_{e0}$ and $\phi \approx \phi_0 + T_{e0} \ell n(n_e/n_{e0})$ along a magnetic field line, where T_{e0}, ϕ_0 and n_{e0} denote integration constants and ϕ is the plasma potential. Typical profiles of ϕ and T_e along the channel centerline are shown in the schematic of Fig 3-left. Thus, though each line is nearly isothermal it is not also of fixed potential unless T_e is zero. This allows for a finite component of **E** parallel to **B** which, in turn, can lead to ion acceleration towards the containing walls if the **B**-lines begin/terminate at the surface of the material. Erosion of the channel walls occurs when ions strike them with sufficient energy to sputter off material.

Deviations from equipotentiality along lines of force near the channel walls has been the main reason that most state-of-the-art (SOA) Hall thruster designs continued to experience channel erosion. To better illustrate the main impediment we use as an example a typical SPT-like magnetic field configuration as depicted in Fig 3-middle. We designate this as a "US configuration." Here the variation of ϕ and T_e along the walls is similar to that along the centerline because the lines are nearly radial. Consequently, the elevated $E_{\parallel}$ and T_e at the walls can drive a flux of high-energy ions to the walls. The induced erosion can be reduced marginally if the curvature of lines is made more convex towards the anode as originally proposed by Morozov *et al*.[18] By comparison, magnetic shielding reduces erosion rates by orders of magnitude in the beginning-of-life configuration of the thruster.

Referring to Fig 3-right, magnetic shielding is achieved by way of a magnetic field topology that sustains high ϕ and low T_e along the channel-grazing magnetic field lines, in fact, as close as possible to V_d and to the coldest values of T_e that can be attained inside the channel, respectively. In this manner the incident-ion kinetic and sheath energies can be marginalized. Moreover, with a properly designed combination of **B** and channel geometry, **E** can be controlled to be both nearly perpendicular to the surface and large in magnitude, as shown in the MS configuration Fig 3-right. In this manner the induced $\mathbf{E}_{\perp}$ forces ion acceleration away from walls without loss of thruster performance. This also reduces the wall-incident ion flux. The key principle behind magnetic shielding lies in the recognition that the electron pressure (yielding $T_e \times \ln(n_e)$ in Eq. (1)) forces **E** and **B** to no longer form an orthogonal set (Fig 3-middle)**.** Thus, a geometry of **B**-lines with convex curvature toward the anode cannot effectively control **E** near surfaces (and, in turn, the erosion) if the near-wall lines are not also equipotential. In contrast, Fig 3-right shows a magnetically shielding **B** topology. This topology eliminates the contribution of the electron pressure by exploiting those **B**-lines that extend deep inside the acceleration channel, near the anode. Because these lines are associated with high ϕ_0 and low T_{e0} the contribution of $T_e \times \ln(n_e)$ is marginalized.

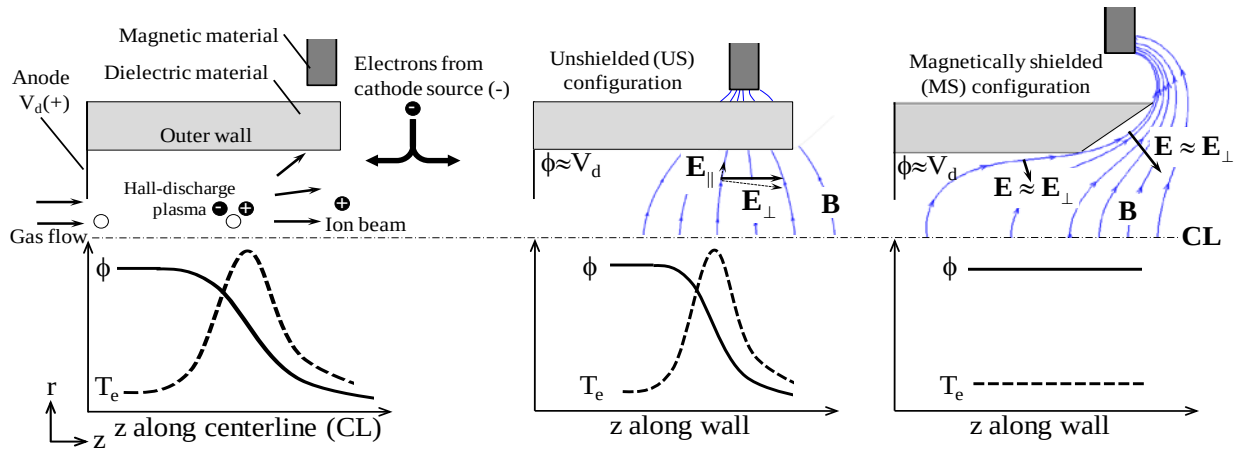

Fig 3. Schematics of the upper half of the annular acceleration channel in a typical magnetic-layer Hall thruster (top) and typical profiles of ϕ and T_e (bottom) established during ion acceleration. Left: Basic features of the accelerator and typical profiles along the centerline. Middle: Representative magnetic field lines and profiles along the wall in a US configuration. Right: Representative magnetic field lines and profiles along the wall in a MS configuration. The line that extends deepest into acceleration channel and runs closest to the channel wall without crossing it is termed the "grazing line."

B. **Computational Model**

The numerical simulations presented in this paper have been performed with the Hall2De code, [4, 19] a two-dimensional (2-D), axisymmetric computational solver of the conservation equations that govern the evolution of the partially ionized gas in Hall thrusters. The governing equations, numerical methodology, various thruster simulations and comparisons with measurements have been presented elsewhere.[4, 15, 16] Here, we provide only a brief overview of the code for completeness and outline recent advancements made to the hydrodynamic model for the ions. For a more detailed description of the new ion algorithms, numerical tests and comparisons with experiments the reader is referred to our companion paper by Ortega & Mikellides.[20]

Excessive numerical diffusion due to the large disparity of the transport coefficients parallel and perpendicular to the magnetic field is evaded in Hall2De by discretizing the equations on a computational mesh that is aligned with the applied magnetic field. Typically, the MFAM spans a computational domain in r-z geometry that extends several times the thruster channel length in the axial direction, and encompasses the cathode boundary and the thruster centerline. In the present simulations the near-plume computational domain spanned approximately 3 and 6 times the acceleration channel length in the radial and axial directions, respectively. The solution of the electron energy conservation equation provides T_e. Ohm's law is solved in the frame of reference of the magnetic field with the electrical resistivity accounting for contributions from collisions of electrons with all other species. It has also been argued that the diffusion of electrons in Hall thrusters is enhanced in a non-classical manner by plasma turbulence.[21-26] In numerical simulations this enhancement has typically been modeled using an effective or "non-classical" collision frequency. Denoting this collision frequency as ν_α, we impose in Hall2De a so-called transport coefficient function $f_\alpha(r,z)$ and set $\nu_\alpha = f_\alpha \omega_{ce}$. Our specification of f_α is guided by plasma measurements whenever they exist. The conservation equations for the electrons are closed with boundary conditions (BC) at all surfaces. The channel (ring) walls are dielectrics emulating the H6 thruster design. For all dielectric-wall boundaries a zero-current condition is imposed. At these surfaces the BC for the convective heat loss follows the formulations of Hobbs and Wesson [27] for the potential drop in a sheath with secondary electron emission. In the H6 the poles are made of iron (Fe). In the simulations presented here, these poles were modeled as dielectric boundaries during the plasma simulation but as conducting boundaries during the erosion calculations, to account properly for the energy gained by ions through the sheath drop in each scenario. Past sensitivity simulations have shown

that though a conducting boundary during the plasma simulation is numerically more oscillatory, on-average the results are very similar. At the anode we impose (conducting) sheath BCs for the electron current density normal to the anode. At the cathode boundary the neutral particle flux, ion flux, plasma potential and electron temperature are specified. The far plume solution is subject to outflow BCs. The energy equation is solved in a semi-implicit fashion; the thermal conduction term is implicit whereas all other terms are evaluated explicitly. Current conservation, incorporating Ohm's law to solve for the electron current density, is also solved implicitly.

The numerical solution of the conservation equations for the heavy species is obtained without invoking discrete-particle methods. The evolution of the (collision-less) neutral species is computed using line-of-sight formulations that account for ionization.[19] Ions are treated as an isothermal, cold (relative to the electrons) fluid, accounting for the drag force and the ion-pressure gradient. The algorithm for the ion hydrodynamics has been completely re-written in Hall2De. The previously explicit, non-conservative, vertex-centered scheme has been replaced with a semi-implicit, conservative, cell-centered scheme that allows for better accuracy and reduced computation times. Inter-cell fluxes are determined using a variant of the Harten-Lax-van Leer (HLL) scheme [28] and is better described in our companion paper. [20] The equations of motion for ions are discretized in time using a semi-implicit predictor/multi-corrector [29] scheme that has shown to reduce Hall2De computation times by 3-4 times.

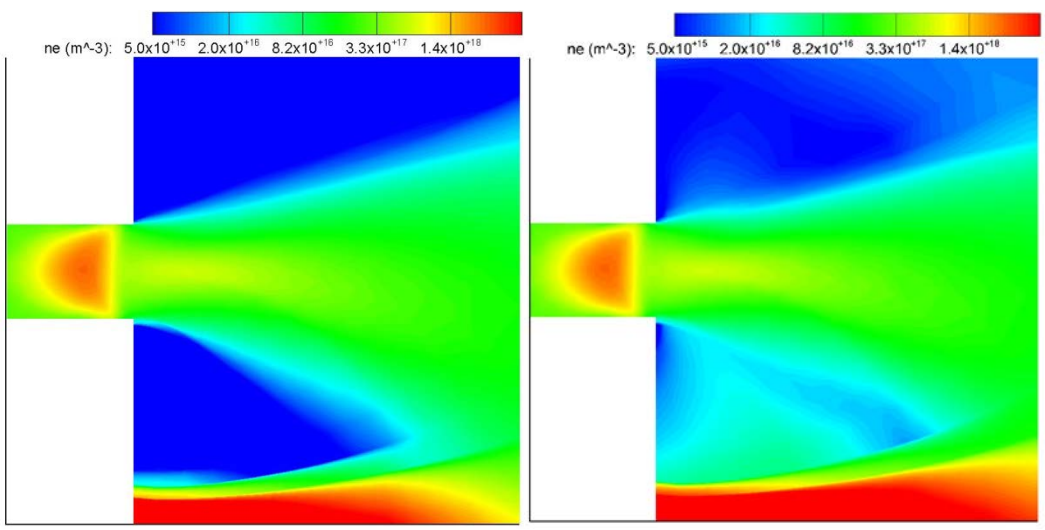

Fig 4. Contour plots of the electron number density from the Hall2De simulation of the H6US. Left: Assuming single ion fluid. Right: Assuming two distinct ion fluids, with E_1=50 V.

One of the principal drawbacks of employing continuum formulations compared to particle methods (like particle-in-cell) for simulating the flow of ions in a Hall thruster is the inability to resolve distinct ion populations. Though the relaxation times for ions can be shown to be small enough inside the acceleration channel, such times can become exceedingly high in the near plume region. Here slow ions from the cathode combined with slow ions generated in this region by ionization and charge exchange collisions have highly disparate transit times compared to the beam ions coming from the acceleration channel. If modeled as a single fluid, convection of slow ions in the near plume will occur at the mean velocity, which is dominated by the momentum of the fast ions. This would in turn result in erroneously low particle densities in regions that reside outside that main beam expansion, such as those near the thruster poles for example.[30] A comparison of the Hall2De solutions for the electron number density with 1 and 2 ion fluids is shown in Fig 4, with the second ion fluid representing ions that were generated at regions where the plasma potential was less than 50 V. Since all previous simulations with Hall2De have focused largely on plasma and erosion physics inside the acceleration channel, the single-fluid approximation has been adequate. However, for pole erosion calculations, a different approach must be followed, as was recognized previously in Hall2De simulations of the BPT-4000.[30]

The novel approach implemented in Hall2De makes use of a multi-fluid algorithm. Determination of the fluid to which a given ion belongs is made upon examining the plasma potential at the location where the ion mass element was generated. Therefore these so-called "threshold" potentials determine the maximum energy $\bar{E}$ at which each ion population is created. So for a total number of N_F fluids, threshold energies are specified in Hall2De as follows:

$$\bar{E}_1 \ldots \bar{E}_i, \bar{E}_{i+1} \ldots \bar{E}_{N_F-1} \tag{3}$$

where the zeroth and N_F^{th} values of $\bar{E}$ are +/- ∞ respectively. Thus in a 2-fluid simulation only $\bar{E}_1$ need be specified. Ions of different populations are created by ionization and charge-exchange collisions depending on how the threshold energy compares to the local value of the plasma potential. The continuity and momentum equations for each fluid i_F with charge i_Z can then be written as follows:

$$\frac{\partial n_{i_Z,i_F}}{\partial t} + \nabla \cdot \left(n\mathbf{u}\right)_{i_Z,i_F} = \dot{n}_{i_Z,i_F} \tag{4}$$

$$\frac{\partial}{\partial t}\left(n\mathbf{u}\right)_{i_Z,i_F} + \nabla \cdot \left(n\mathbf{u}\mathbf{u}\right)_{i_Z,i_F} = \mathbf{R}_{i_Z,i_F} - m^{-1}\left(n_{i_Z,i_F} q_{i_Z} \nabla\phi + \nabla p_{i_Z,i_F}\right) \tag{5}$$

where n is the number density, **u** the fluid velocity, p the pressure, ϕ the plasma potential, q the charge, m the atomic mass, $\dot{n}$ the rate of gain/loss of ions through ionization and charge exchange, and **R** the momentum-exchange or drag force, consisting of contributions from elastic and inelastic collisions. A more detailed description of the formulation, numerical implementation and testing is presented by Ortega & Mikellides.[20] It should be noted that as part of testing the fidelity of the multi-fluid algorithm, Katz and Ortega also developed and implemented a PIC algorithm for ions in Hall2De. Numerical tests showed that the 2-fluid hydrodynamic solution was very close to the PIC solution in the near-plume. It was also shown that the addition of a third ion fluid did not alter the results significantly.[20] Therefore all simulations performed here to assess pole erosion have been conducted assuming two distinct ion fluids. Up to triply charged ions are accounted for each of the two fluids yielding a total of 6 ion momentum equations.

C. Simulation Results and Comparisons with Plasma Measurements

The advancements made to the ion hydrodynamics have undergone extensive numerical testing and sensitivity analyses. The results of these tests along with comparisons with plasma measurements are reported in our companion paper by Ortega and Mikellides.[20] Here we present a representative set of comparisons with measurements taken in both the H6US and H6MS thrusters to illustrate the state of the code's fidelity, and to identify uncertainties. Though the computational plume region extends several channel lengths L downstream of the thruster exit, we show in Fig 5 only a closer view of the regions that are relevant to the present work. Both the H6US and H6MS geometries are shown for comparison. Also shown are the basic locations of the poles in the two configurations relative to the acceleration channel. Noted are the chamfered portions of the channel in the H6MS, a characteristic feature of MS thrusters, and the fact that in both configurations the axial location of each pole surface facing the plasma is not the same as the axial location of the channel exit plane. In both thruster configurations the poles are in fact at a small distance behind the exit plane. The distances from the thruster centerline to the outer radius of the inner pole and to the channel centerline are denoted by R_o and R, respectively. In the simulations presented here this gap is not modeled. The wall boundaries representing the poles are taken to be at the same plane as the channel exit plane; the cathode boundary is also located along the same plane. The implications of this assumption are discussed in detail in Sec. III. All results presented hereinafter have been produced for the 300-V, 6-kW (20-A) operating condition [3], under vacuum conditions unless otherwise stated.

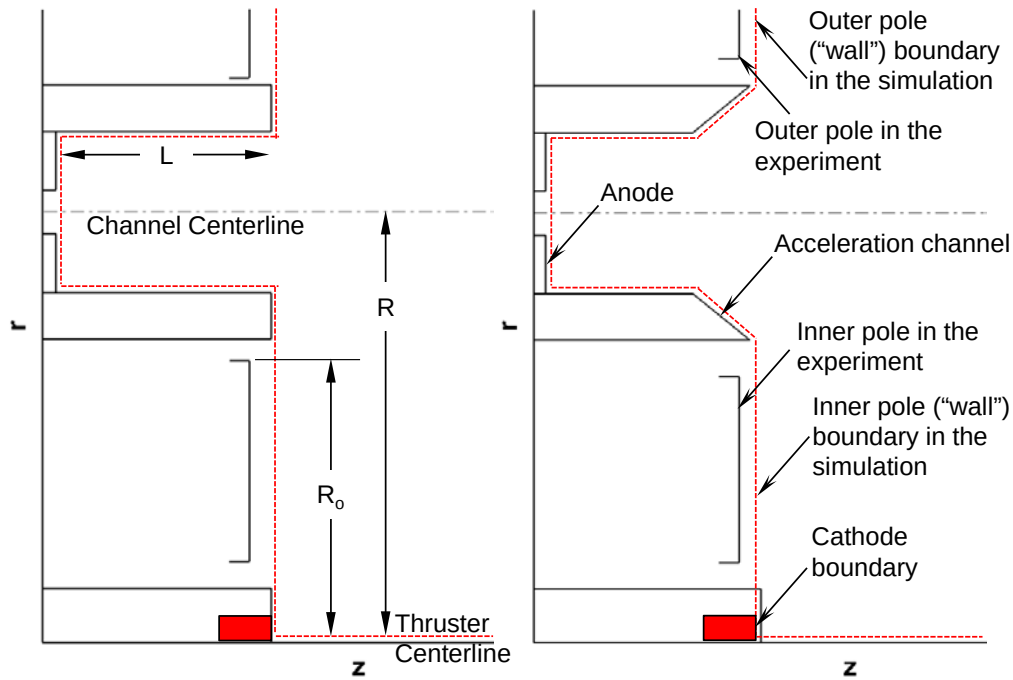

Fig 5. Schematics of the channel and inner pole regions in the H6US (left) and H6MS (right) configurations showing location of the poles. Also shown by the colored dashed outline is the computational region defined for the numerical simulations with Hall2De.

1. <u>H6US Configuration</u>

All simulations have been performed assuming two ion fluids with $\bar{E}_1$=50 V. The choice of 50 V as the threshold energy distinguishing the two fluids is based on several sensitivity simulations that indicated this value best represents the plasma properties in the regions of interest, based on all the available plasma measurements. Figure 6 compares computed (left) and measured (right) discharge current oscillations. We found that the computed frequency and pea-to-peak values are 13 kHz and 4.7 A respectively, compared to 14 kHz and 5.9 A measured during nominal operation of the H6US in a vacuum facility. The low-frequency plasma oscillations in the Hall2De simulations have been found to be closely coupled to the cathode, which unlike HPHall [31, 32] and other similar codes [33, 34] that employ smaller plume regions, encompass the cathode boundary at its real location on the thruster centerline. This close coupling between thruster and cathode and the effect of the background gas on theses oscillations is currently being investigated more thoroughly.

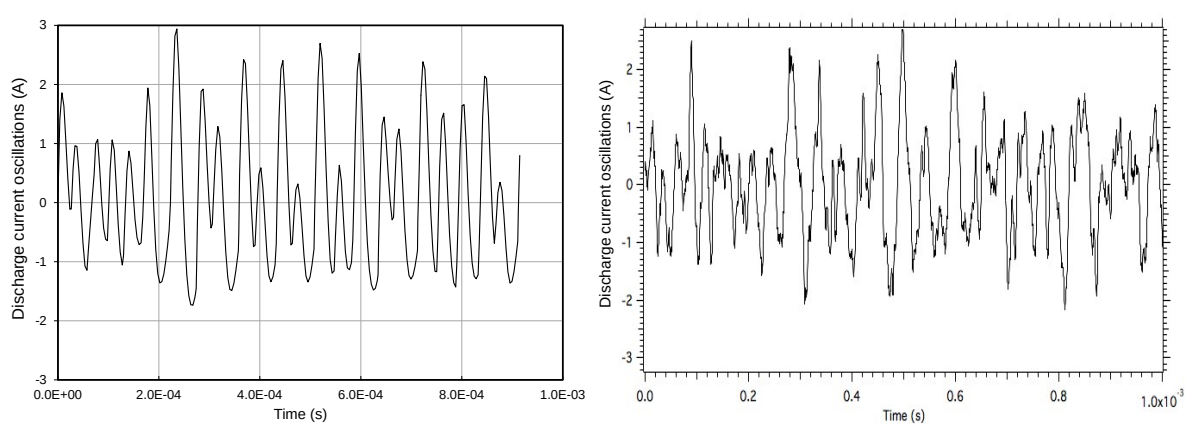

Fig 6. Comparison of the measured (left) and computed (right) discharge current oscillations for the H6US. (Values are presented as the mean minus the instantaneous values of the discharge current.)

Time-averaged results and comparisons with plasma measurements are illustrated in Fig 7. The left plot shows contours of electron number density pointing to two locations, z/L=1.19 and r/R=1 at which all ensuing comparisons will be presented. Location r/R=1 is the channel centerline. The right plot depicts our most recent comparisons for the computed electron temperature and plasma potential. Experimental results from two sets of measurements also are presented. Measurements using fast-scanning probes are termed "injected probes" in the plots. These probes spanned both the near-plume and the channel interior.[3] Because it has long been suspected [35, 36] that these methods may be invasive in Hall thrusters, a recent focused investigation performed at JPL demonstrated that the interior plasma is indeed perturb by the presence of the scanning probe.[37] The same investigation showed that the near-plume plasma, up to approximately the channel exit, remains relatively un-perturb. The results of these investigations are currently being prepared for publication. In light of these latest results we have chosen to exclude from our comparisons the injected-probe measurements in the channel interior. Instead, in the interior, we use wall probe data for the electron temperature that have been extrapolated onto the channel centerline along magnetic field lines. The extrapolation is valid since the isothermality of the lines in the channel interior has been confirmed experimentally.[2] In the near-plume we continue to use the injected-probe data. We show two sets of such measurements in Fig 7, taken in 2012 and 2014, to illustrate the extent of possible variations from one set of measurements to another. Though still within the experimental error (which includes variations from one measurement to another), we find that the simulations compare well with the electron temperature measurements in the near plume but underestimate them in the interior by as much as ~ 7eV (~20%).

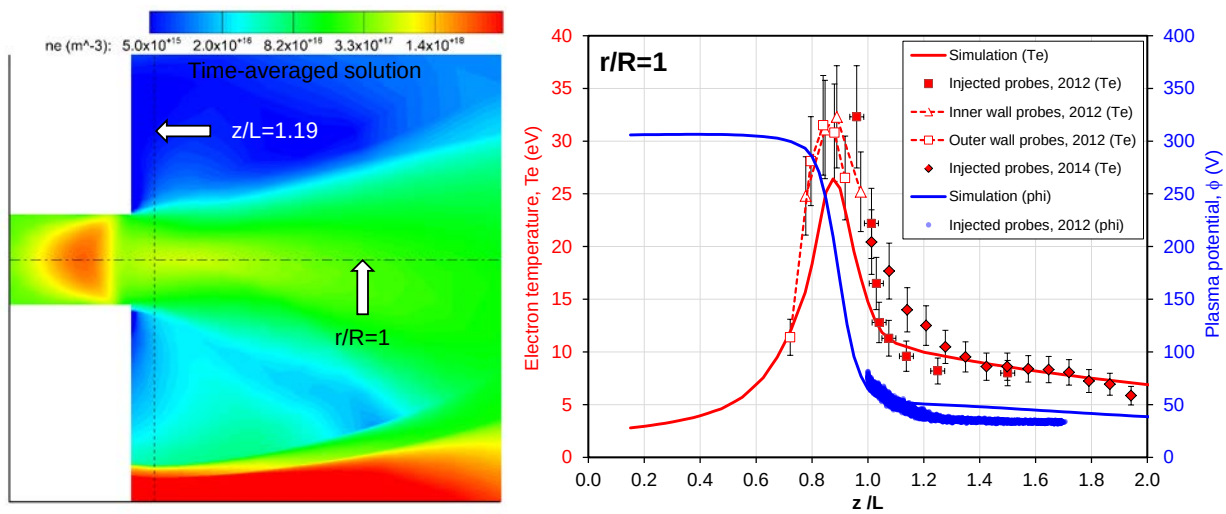

Fig 7. Left: Contour plot of the time-averaged electron number density in the H6US showing slices along which several comparisons are presented throughout this paper. Right: Comparison of computed and measured plasma properties along the channel centerline (r/R=1). Most measurements were obtained during tests in 2012.[3] The electron temperature measurements using scanning probes were repeated in 2014 in the same vacuum facility (unpublished).

The plasma potential in the near-plume compares well with the measurement at the channel exit but the results begin to deviate somewhat downstream of this location. The radial measurements were taken with scanning probes in 2008,[38] when the thruster was operated at about a 6% higher value of the anode flow rate than in the 2012 experiments and in the simulations that are presented here. The radial comparisons at z/L=1.19 depicted in Fig 8 show that the plasma potential at the channel centerline is over-predicted in the simulations by about 22% but under-predicted by about 33% at r/R=0.5. The total ion current density compares very well with the measurement in the beam and deviates to about a 70% lower value at r/R=0.5. Our simulations have shown that in this region of the thruster, the cathode plume is dominated by classical collisions; that is, no "anomalous" collision frequency is needed. This was

determined upon observation that the steep gradient that is evident near the thruster centerline in the plasma potential measurement (Fig 8) could not be reproduced by the simulation if the anomalous collision frequency model we employ extended to encompass the cathode plume. We hypothesize that the absence of anomalous transport here may be driven by enhanced collisional damping of the turbulence, enabled by the high plasma density produced by the cathode (10^{18}-10^{20} m^{-3}). We have also found that the discrepancy between simulation and experiment is sensitive to small variations in the classical collision frequency, namely factors of ~2 from the range of values presently computed. Such variations can be due to a range of causes including differences in the collision cross sections for the electron-neutral collisions, in the boundary conditions defined for the electrons temperature at the cathode, the far-plume boundary and the background pressure, and/or due to the higher anode flow rate used in the 2008 measurements. These sensitivities continue to be investigated but are beyond the scope of this work.

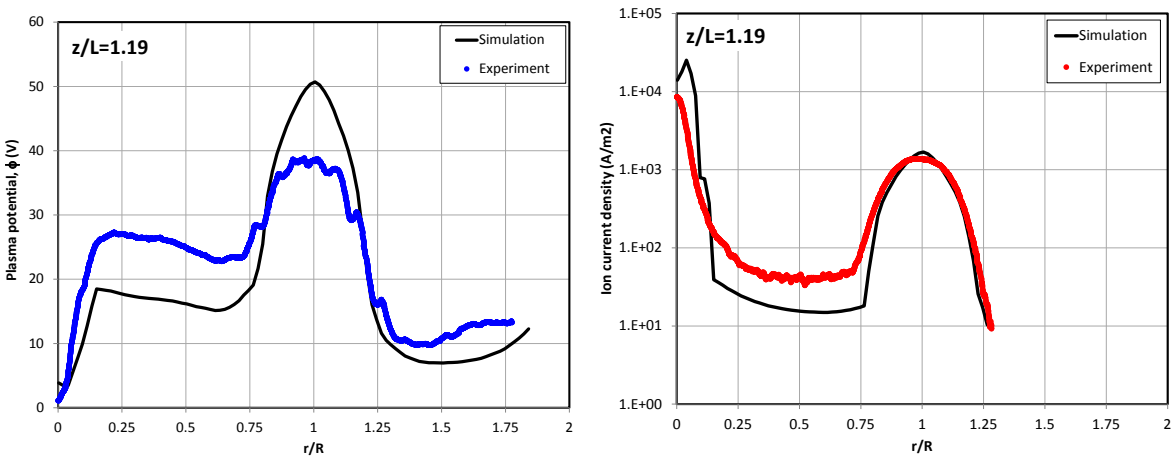

Fig 8. Comparison of computed and measured properties along a radial slice at z/L=1.19. Left: Plasma potential. Right: Total ion current density. The measurements were obtained in 2008.[38]

2. <u>H6MS Configuration</u>

The numerical simulations for the magnetically shielded thruster have been performed using also two ion fluids, with $\bar{E}_1$=50 V. The differences between the H6US and H6MS in terms of operating conditions, magnetic field, and simulation specifications have been outlined in previous publications.[2, 3, 8] It should be noted here that the profile f_α of the anomalous collision frequency in the H6MS is found to be, in general, different than that in the H6US. In the present simulations it has been specified based on guidance from the plasma measurements. The computed electron number density contours and the comparison between simulation results and plasma measurements along the channel centerline are plotted in Fig 9. The results at the channel centerline are plotted as a function of z/L_{MS} where L_{MS} is the channel length of the H6MS, which is slightly smaller than L. The same fast-scanning probe arrangement that was used in the H6US was used also in the H6MS to produce the measurements in Fig 9-right. Thus, due to the same reasons associated with probe perturbations of the interior plasma, only the near-plume data are presented. Unlike the H6US however, data from wall probes installed in the H6MS cannot be extrapolated to the centerline since no magnetic field line intersects both the wall probes and the centerline (e.g. see Fig 3, right). The comparisons show overestimated values in the simulation downstream of the exit plane, by about 45% for the electron temperature and 30% for the plasma potential at z/L_{MS}=1.5. However, near the z/L_{MS} =1 plane where the pole erosion calculations have been performed, the simulation results are within 10% of the measurement. Data from radially scanning probes are not yet available.

Noted in Fig 9-left are the characteristic low-density regions (<10^{15} m^{-3}) surrounding the channel corners at the exit plane. Unlike unshielded thrusters, these regions persist in magnetically shielded thrusters due to the structure of the plasma potential near these corners. More specifically, the

convergence of magnetic field lines here forces a high electric field which in turn accelerates rapidly most ions that made it there from the channel interior and any ions that were created here. This feature in magnetically shielded thrusters is favorable because these high energy ions are predicted by the hydrodynamic formulations to be expelled away from walls and are therefore not expected to cause any erosion. However, sheath effects, which cannot be captured self-consistently around these corners by the ion hydrodynamics in Hall2De, may alter this potential structure here. This is discussed further in Sec. III.

Until this point all simulations have assumed no background pressure. We attempt here to assess the significance of background neutrals on our results. We do so by allowing neutrals that are uniformly distributed along the outer boundaries of the computational domain at number density n_n to enter the domain at the average random thermal flux of $n_n c/4$, where c is the mean atomic speed. The neutral gas density has been determined based on the value of 1.7e-5 Torr, the background pressure that was measured during the H6MS experiments. We note that by assuming a uniform neutral gas density along the outer boundaries the contribution of atomic species from the facility inside our computational domain is overestimated. This is because in reality a significant amount of background neutrals is depleted inside the main beam by ionization with electrons and charge-exchange with ions. Presently, our computational domain is not large enough to extend the outer boundaries to a location where the assumption of uniform gas density is valid. Therefore plume simulations employing a new plume code developed by Ortega and Katz,[39] is being used to better assess gas depletion near the Hall thruster. The plume code uses the results of the Hall2De simulation as the plume boundary conditions to compute the expansion of the plasma. We plan to report the results of the calculations on the neutral gas depletion, combined with a more extensive assessment of background pressure effects on the thruster performance and life, in a future publication. In the present simulations we proceed with the overestimated values of the neutral gas density inside the Hall2De domain to obtain a preliminary assessment of the effects of the background neutral gas on our calculations of pole erosion. The solution with backpressure (BP) for the plasma potential and electron temperature along the channel centerline is plotted in Fig 9-right. We find negligible differences with the measurement in the latter and better agreement in the former in most of the near plume region for which a potential measurement exists. In fact, a closer look at the results along z/L=1.19 shows that the two solutions (w/ and w/o BP) bound the measurement; in the case w/o BP the measurement is overestimated by ~25 V whereas in the case w/ BP it is underestimated by ~12 V. Radial measurements in the H6MS are not yet available but are planned for the near future.

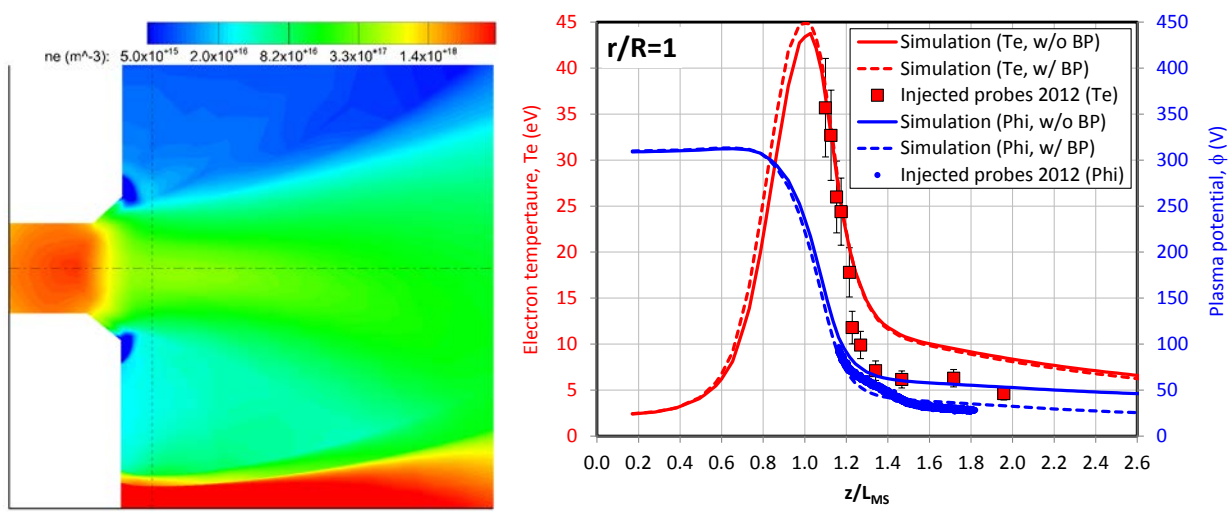

Fig 9. Left: Contour plot of the time-averaged electron number density in the H6MS. Right: Comparison of computed and measured plasma properties along the channel centerline (r/R=1). All measurements were obtained during tests in 2012.[3]

A comparison of the computed neutral gas density along the z/L=1.19 radial slice is plotted in Fig 10-left. The regions that are mostly affected by the background neutral gas are clearly seen on the plot. We find the thruster neutral density to be as much as ~3-5 times lower than the background density in regions where r/R≤1; even larger differences occur at larger radii. Due to the reduction of the plasma potential however and the increasing rate of charge-exchange collisions in these regions, we find ions to be of lower energy. In Fig 10-right we compare the total energy of Xe^+ striking the inner pole wall boundary ($z/L_{MS}=1$). This value consists of both the energy ions have gained through plasma before entering the sheath and the sheath energy. In fact, in the regions of enhanced gas density due to background neutrals we find the ion energy to be below the sputtering yield threshold for iron (Fe) which we estimate to be ~8 V. (The erosion and material models are further discussed in Sec. II). It is therefore possible that the background neutrals have a lesser effect in these near-pole regions of the thruster than what is suggested by the simulations w/ BP, assuming no depletion of neutrals around the outer boundaries of the Hall2De domain. A closer investigation on background pressure effects, using a combination of numerical simulations and dedicated experiments, is currently underway and is planned for publication in the near future. In this paper, we proceed to present preliminary results with the plasma solutions for the H6US and H6MS in the absence of backpressure.

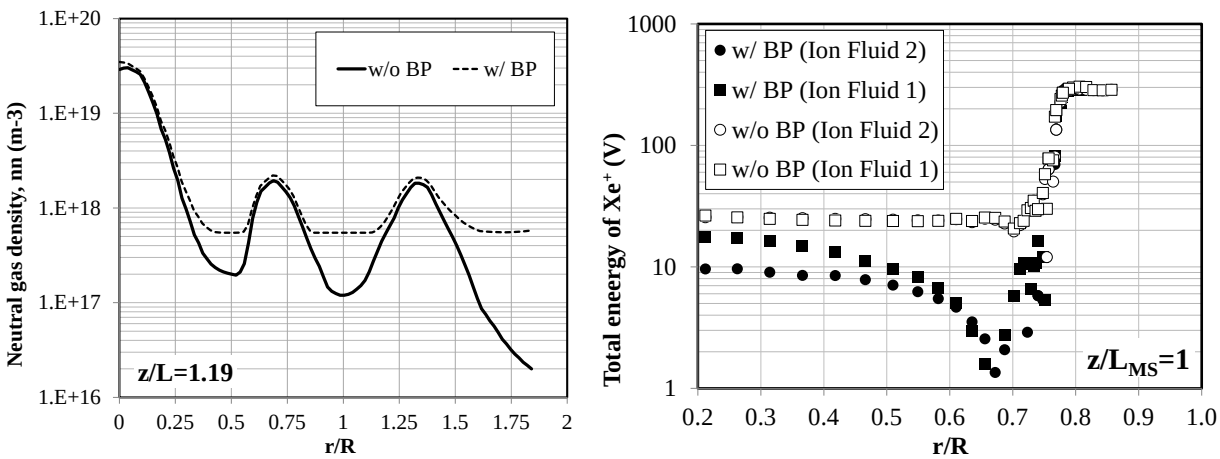

Fig 10. Left: Computed neutral gas density along a radial slice at z/L=1.19 in the H6MS comparing solutions with and without backpressure. Right: Computed energy of singly-charged ions striking the inner pole wall boundary in the simulations in the two cases, with and without backpressure.

Contours of the computed plasma potential in the H6US and H6MS configurations are compared in Fig 11-top. Noted is the distinctively different structure of the plasma potential near the exit of the two configurations. These regions have been compared and discussed in detail in previous articles.[1, 2] Figure 11-middle depicts contours of the fluid-1, Xe^+ representing largely the main-beam ions. Also shown on the same plot is the vector field of Xe^+ current density. The comparison shows a larger divergence of the H6MS ion beam compared to that of the H6US. This is expected because (1) the acceleration region is located further downstream than that in the H6US and (2) the more curved magnetic field topology of the H6MS near the chamfered channel walls leads to a plasma potential structure with a more concave distribution in the near plume. These two effects also lead to the distinctively different current density vector fields of the fluid-2 ions shown in Fig 11-bottom, which represents ion populations generated at potential less than 50 V. Specifically, it is found that these ions along the inner pole wall boundary in the H6MS have a higher incidence angle compared to that in the H6US. The possibility of enhanced erosion by the flow of these slow ions towards the inner pole is assessed in the next section.

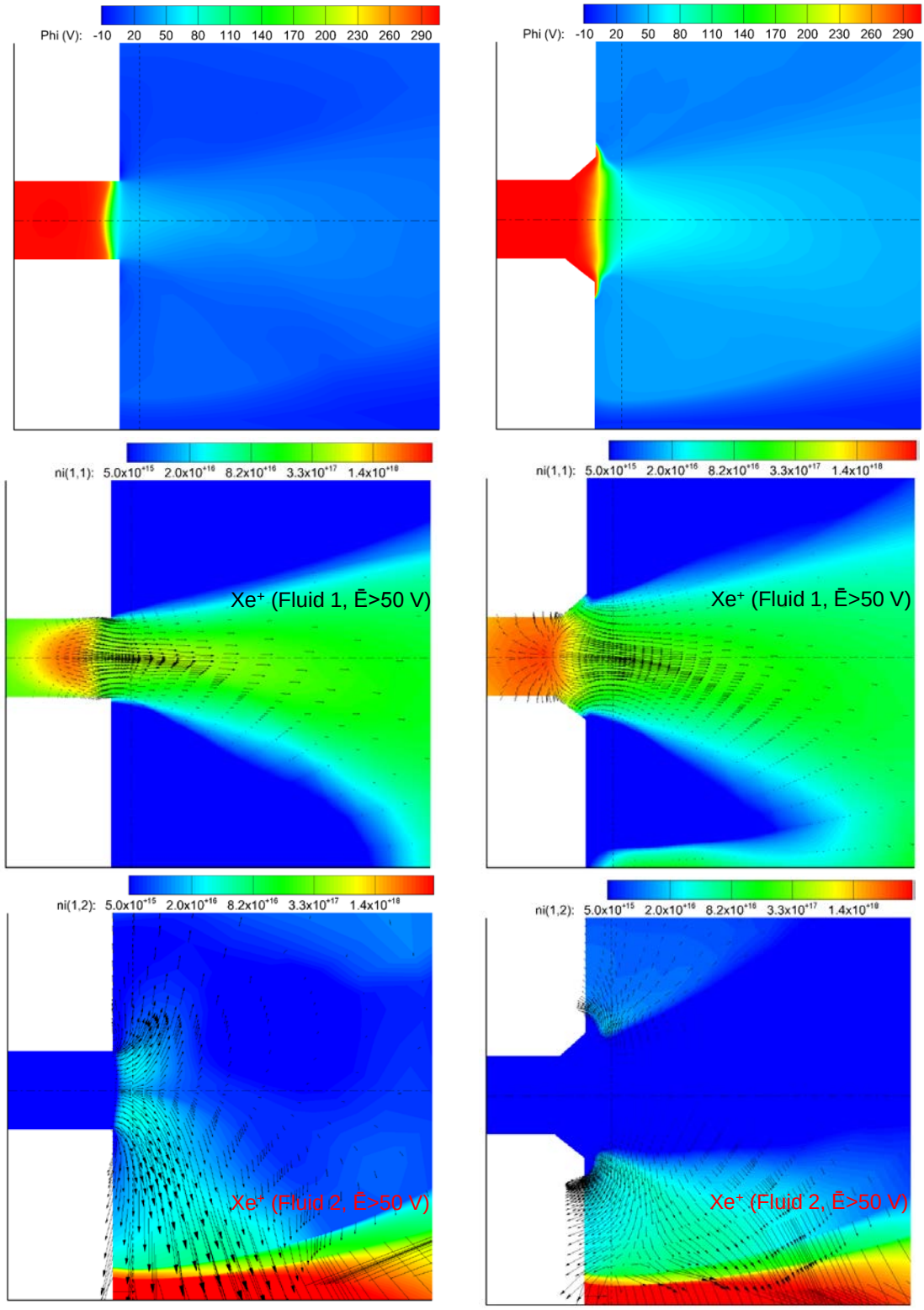

Fig 11. Computed time-averaged plasma parameters in the H6US (left column) and H6MS (right column). Top: Contours of the plasma potential. Middle: Number density contours and current density vector field of the Fluid-1, singly-charged ions. Bottom: Number density contours and current density vector field of the Fluid-2, singly-charged ions.

II. Inner Pole Erosion Assessments

A. Erosion Model

Erosion in Hall2De accounts for contributions from three charge states, Xe^{+}, Xe^{++} and Xe^{+++}, for each ion fluid. The sputtering erosion rate (ε) due to ion bombardment by ions of charge state i_Z and fluid state i_F is given by,

$$\varepsilon_{i_Z,i_F} = j_{i_Z,i_F} Y \tag{1}$$

where the incident ion current density perpendicular to the channel wall, j_{i_Z,i_F}, is dependent on the ion number density (n_{i_Z,i_F}) and the ion velocity (u_{i_Z,i_F}) at the wall. The sputtering yield of the channel material, Y, is a function of the ion impact energy K and incidence angle β. Y is expressed throughout the paper in mm^3/C unless otherwise noted. The total erosion rate is the sum over all fluids and all charge states:

$$\varepsilon = \sum_{i_Z=1}^{N_z} \sum_{i_F=1}^{N_F} \varepsilon_{i_Z,i_F} \cdot \tag{2}$$

Because ions must traverse a sheath before striking the wall, the total impact energy is the sum of the kinetic energy ions have acquired in the plasma upon entrance to the sheath, and the sheath potential energy. The potential energy, transformed to ion kinetic energy as the plasma ions are accelerated inside the sheath towards the solid material, is computed based on the Hobbs and Wesson solution to the 1-D sheath equations in the presence of secondary electron emission. [40] In the numerical simulations the edge-centered ion velocity and the element-centered ion number density at each computational element adjacent to the wall boundary are used to determine the total impact energy, $K=K_{plasma}+K_{sheath}$, and angle β. Then the sputtering yield is determined as follows:

$$Y = f_\beta(\beta) f_K(K) \tag{3}$$

where $f_\beta(\beta)$ and $f_K(K)$ are fitting functions for the angle and energy dependence at zero angle of incidence, respectively. The material of the thruster poles is largely Fe. Sputtering yield measurements for Xe on Fe in the range of 100<K<600 V were taken by Rosenberg and Wehner,[41] and are plotted in atoms/ion in Fig 12-left. Also potted in Fig 12-left for comparison are the data for molybdenum (Mo) by Doerner et al.,[42] which extend to much lower ion energies than the data for Fe. For boron-nitride (BN), we have been using a model by Bohdansky [43] to extrapolate Y from the available data at K>100 V to lower ion energies, as shown in Fig 12-right. The ion energy threshold for BN in the case plotted is 35 V. However, we have found that Bohdansky's model fails to capture the variation of Mo at K<100 V for which data do exist. We have therefore proceeded to use a least-squares best fit to the Mo data to capture the variation of the sputtering yield of Fe for K<100 V. Also shown is a best fit to carbon (C) sputtering yield data obtained by Doerner, et al.,[42] that will be discussed further in Sec. III. No published data were found for the angular dependence of Xe on Fe and C so we have incorporated the same function as that used for BN. The fitting functions we have used are as follows:

$$\begin{aligned} f_\beta(\beta) &= \cos(\beta)^{-c_0} \exp\left[-c_1\left(\cos(\beta)^{-c_2} - 1\right)\right] && \text{(a)} \\ f_K(K) &= A \exp\left[B + \frac{C}{\left(c_3 \ell n(K) - c_4\right)^{c_5}} + D \exp(c_6 K)\right] && \text{(b)} \end{aligned} \tag{4}$$

The coefficients used in Eq (4b) are tabulated in TABLE. We note that the fit for the energy dependence yields an ion energy threshold of ~8 V for Fe. In the Hall2De code ε is set to zero when the ion energy is less than the threshold value.

Table 1. Coefficients in the sputtering yield fitting function $f_K(K)$ in Eq. (4b).

	A	B	C	D	c_0	c_1	c_2	c_3	c_4	c_5	c_6
Fe	0.185	8.101	-38.744	0	2.5204	0.8552	1	4.3429	9	0.5	0
C	0.055	7.788	-57.383	-147.94	2.5204	0.8552	1	1	0	1	-0.09

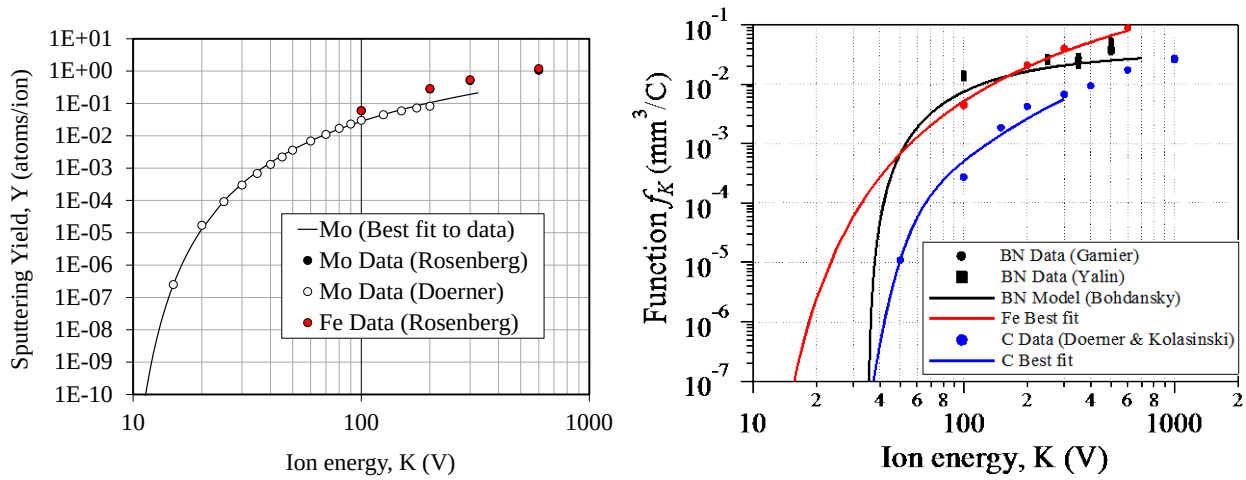

Fig 12. Sputtering yield as a function of ion energy at zero angle of incidence. Left: Measurements for Mo and Fe (in atoms/ion). Also shown is a best fit for Mo. Right: Measurements and fits for BN, Fe and C (in mm^3/C).

B. **Erosion Results**

The plasma solutions for the H6US and H6MS presented in Sec. I and the material information presented in Sec. II.A have been used to determine the erosion rates of the inner pole. We note here that a main reason for computing also the erosion rates in the H6US, even though minimal or no roughening of the pole surface was observed in this configuration, is to allow for a direct comparison with the H6MS results at the same material properties. This is important in light of the large uncertainties associated with these properties, especially in regards to the sputtering yields at ion energies <100 V. The computed total ion energy bombarding the inner pole surface is plotted in Fig 13-left for both thruster configurations. We plot here only the energy of the slow-born (fluid-2) Xe^+ since we have found that they are the ones with the larger contribution to the erosion rate. Also shown for reference is the value of r/Ro in each thruster configuration to indicate the location of the outer radius of the inner pole. As expected, based on the computed plasma potential (Fig 13-left), the energy of ions K along the entire inner pole in the H6US simulation does not exceed 40 V. The energy of fast-born (fluid-1) ions begins to increase as r/R approaches unity but their flux is negligible compared to the fluid-2 ions along the entire pole. On the other hand, the characteristic feature of the plasma potential exhibited in the H6MS near the downstream exit corner of the chamfered portion of the channel, leads to much higher energies for r/R>0.7 reaching the discharge voltage at ~r/Ro. The "leakage" of high plasma potentials in this corner is a consequence of the magnetic field topology in this area and is a commonly-observed feature in hydrodynamic simulations of magnetically shielded thrusters. The argument against any significant erosion caused by this feature has been that in this region the ion density drops significantly due to the radial expansion of the main

beam, thus the flux that can bombard the surface is low. Further expansion of the ions due to the high electric field that forms along the pole surface directs ions away from the poles thereby further reducing the flux of high-energy ions that can strike the walls. It is recognized however that this is based on hydrodynamic arguments and, naturally, does not take into account in a self-consistent manner the presence of the sheath since its formation cannot be resolved by Hall2De. This is discussed further in Sec. III.

The computed erosion rates for the two configurations, assuming an Fe-pole, are plotted in Fig 13-right. We find the expected increase in erosion rate in the H6MS for r/R>0.7, peaking to a value of 1.7e-2 mm/kh at r/R=0.75. This is approximately 4.5 times higher than the deposition of carbon and other sputtered deposits. As we discussed in previous publications, since the effective sputtering yield of materials that have been covered by layers of deposits is in principle different than that of the original material, we can only suggest without proof that this region of the pole could exhibit some roughening due to sputtering. A roughened strip around this region of the outer pole was indeed observed after the 150-h wear test, as shown in (Fig 2-right). However, the inner pole was observed to exhibit evidence of roughening throughout most of its area. Yet, other than the region r/R>0.7, the computed results do not support this observation. The erosion rates are found to be below the deposition rate and comparable to the H6US which did not exhibit any evidence of sputtering. Possible reasons for this discrepancy are discussed in the next section.

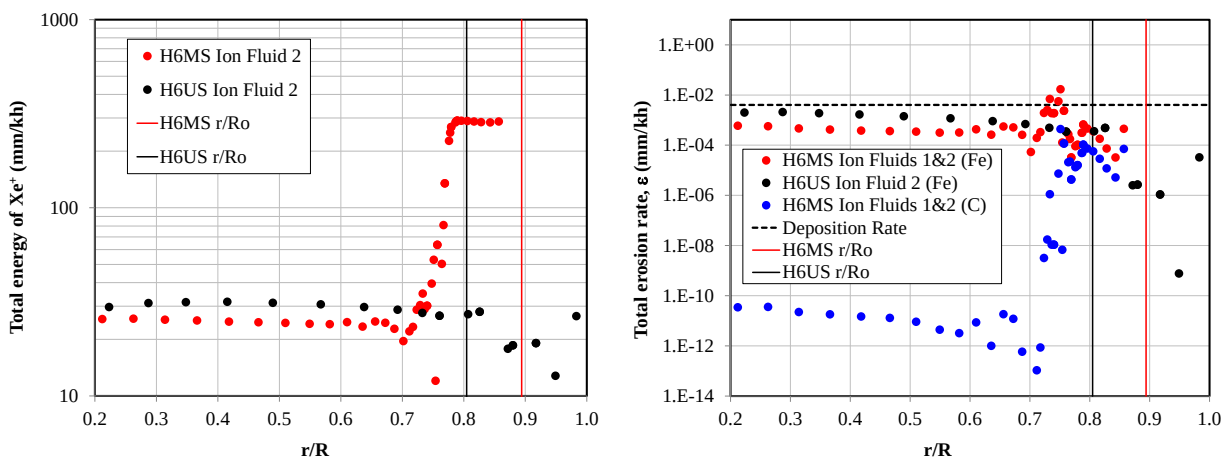

Fig 13. Left: Comparison of the total energy of singly-charged ions striking the inner pole wall boundary as determined by the Hall2De simulations. Right: Comparison of the computed erosion rates in the two thruster configurations assuming the inner pole is made of Fe or C. Also shown for reference is the location of the outer radius of the inner wall pole in each thruster configuration.

III. Discussion

The hydrodynamic solution from the simulations of both configurations suggests the following picture regarding the expansion of ions around the channel corners. Referring to Fig 14-left, ions associated with main beam in the H6US gain mostly axial velocity inside the acceleration region which is located just upstream of the channel exit. The acceleration region here is formed by a potential structure that is slightly convex relative to the anode due largely to the shape of the magnetic field lines there. As such, main-beam ions are directed away from the exposed inner wall boundary. This picture is illustrated by the contour plot in Fig 14-left, overlaid by a few representative magnetic field lines. In the H6MS configuration on the other hand the specific curvature of the magnetic field topology that must be established around the chamfered channel regions to protect these walls from erosion, forces the maximum magnetic field along the channel centerline to be located downstream of the same point in the H6US. Consequently, the acceleration region in the H6MS occurs further downstream compared to that in the H6US. This is better illustrated in Fig 14-right. Then the curvature and coalescence of magnetic field lines to the inner-pole "wall," combined with the forward location of the acceleration zone relative to the

exit plane produce the characteristic "leakage" of the plasma potential that is observed in the simulations. In this region along the inner pole wall boundary the hydrodynamic simulations yield an electric field that directs most low-density, high-energy ions that make it here from the main beam, or ions generated inside this region, away from the boundary as illustrated in Fig 14-right. This result is supported by the computed ion energies and erosion rates in Fig 13. Though some ions with K>100 V do strike the surface, their densities are not found to be high enough to cause any significant erosion; the maximum computed erosion rate is found to be 4.5 times higher than the measured deposition rate of carbon and other sputtered materials.

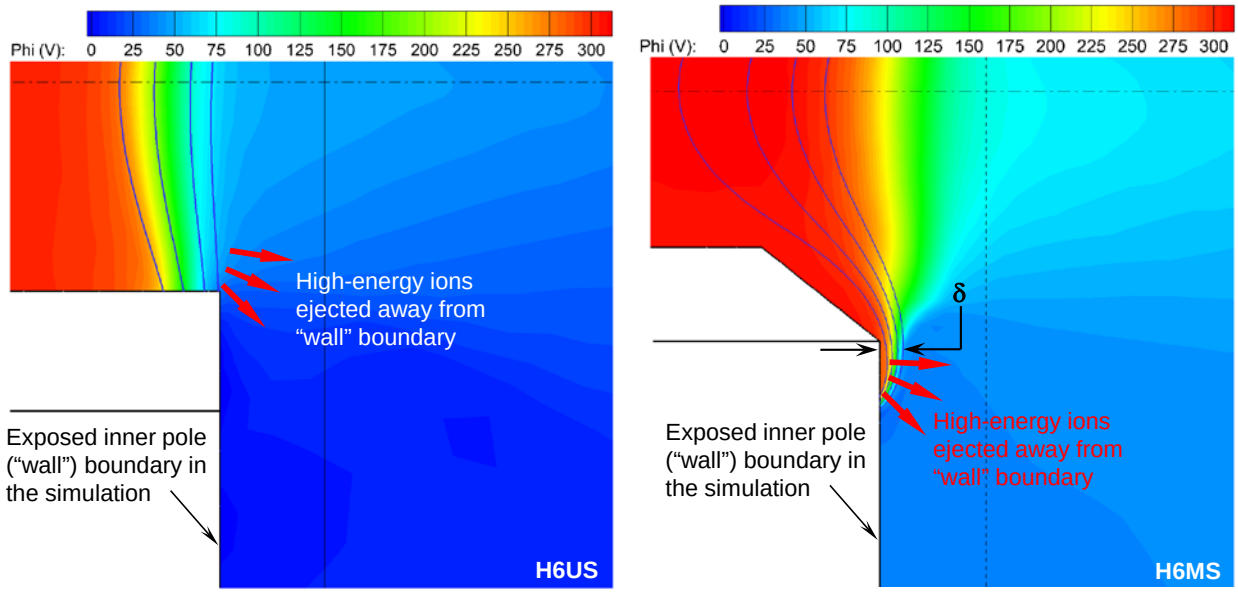

Fig 14. The computed plasma potential in the H6US (left) and H6MS (right) in the channel and near the inner channel corners. Noted are the distivlely different structures of the potential contours at the two corners.

As alluded to earlier, the structure of the leaked potential in the corner of the chamfered region in the H6MS is directly linked to the magnetic field curvature there which, as shown in Fig 14-right, intersects the "wall" boundary at impact angles that are much less than 90 degrees. This is true in the simulations because the wall boundary has been taken to be at the same axial location as the exit plane. Referring to Fig 15, in reality the H6MS inner pole is located $\Delta z/L_{MS}$=0.054 upstream of the exit plane which allows for the magnetic field lines to form naturally along the pole at angles of ~90 deg. This is illustrated in the schematic of Fig 15-left. We argue then that in the wear test of the H6MS the magnetic field topology allowed the leaked potential to curve around the corner yielding higher angles of the electric field vector relative to the pole plane and, in turn, ejection of high energy ions also at higher angles. This would have led to a higher concentration of high-energy ions striking the pole and higher erosion rates. Since the computed erosion rates for r/R<0.7 are only factors of 7-15 lower than the deposition rate, it would not take a significant amount of ions to increase the rate to comparable values. Figure 16 plots the number density of Xe^+ as a function of energy that would be required to raise the computed rates to the measured deposition rate. For reference, the density in the region 0.7>r/R>1 near the pole varies by about three orders of magnitude (~10^{12}-10^{15} m^{-3}) as shown in Fig 16-right. The plasma potential falls by more than 200 V in this region.

If the possible explanation behind the observed roughening of the poles (Fig 2-right) that is proposed here is true then a mitigation technique can be incorporated with relative ease. Graphite coating of sufficient thickness such that its front surface is at the same plane as the exit plane would expose it to ion bombardment that is commensurate to the results of the Hall2De simulations. Combined with the lower sputtering yield of graphite, the erosion rates could then be reduced by as little as 41 times to as much as

~8 orders of magnitude, as shown in Fig 13-right. The maximum erosion rate with the graphite coating is found to be 4.4e-4 mm/kh. At this rate, the full coating at this location would be eroded away after thousands of kh which is many orders of magnitude more than the life requirement for ARM. We also note that this maximum rate of 4.4e-4 mm/kh is subject to significantly less uncertainty associated with the sputtering yield since at this location of the surface the energy of ions striking it is ~65 V. This value is close to the 100-V mark for which the first measured value of the sputtering yield of C exists (see Fig 12-right).

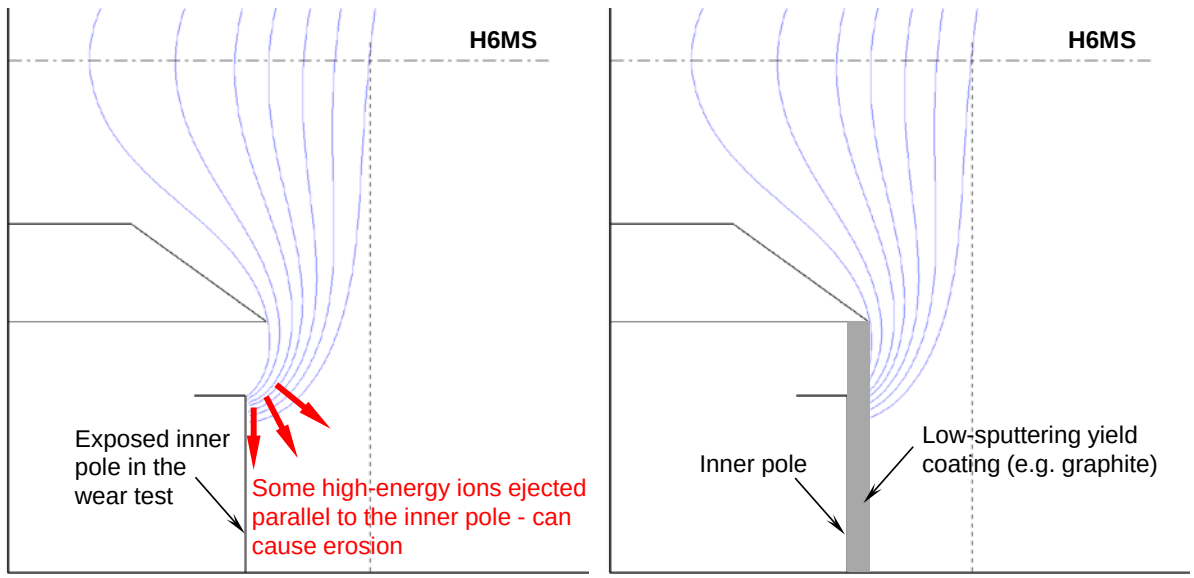

Fig 15. Schematic of the region near the chamfered channel walls of the H6MS showing a set of representative magnetic field lines. Left: current thruster configuration suggesting potential for ejection of high-energy ions at higher angles due to the normal incidence angle of magnetic field lines at the poles. Right: Proposed thruster configuration showing graphite coating. This configuration emulates the geometry constructed in the numerical simulations which suggested erosion rates comparable or lower that the measured depositions rate. The lower sputtering yield of graphite could yield erosion rates that are 41 to 8 orders of magnitude lower.

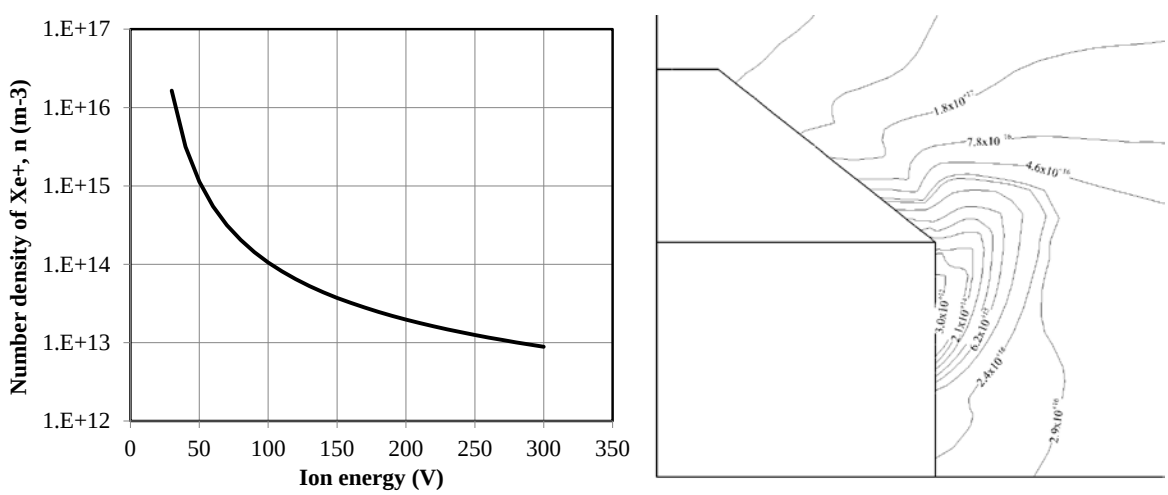

Fig 16. Number density of singly-charged ions that would be required at a given ion energy to raise the existing value of the computed erosion rate of the Fe-pole (Fig 13-right) in the H6MS to the measured deposition rate. Right: Computed number density of singly-charged ions (in m^{-3}) in the vicinity of the H6MS chamfered channel inner wall.

It should be recognized here that, though plausible, the abovementioned mechanism has been proposed without quantitative evidence. To emulate the actual thruster configuration (Fig 3), Hall2De simulations with a retracted inner pole "wall" boundary would have to be performed. Such simulations would be challenged by the failure of the continuum assumption behind Hall2De's hydrodynamic formulation since the ion densities would drop even more precipitously around the corner in this arrangement. In fact, the computed conditions of the plasma near the inner corner of the H6MS channel already challenge the continuum assumption. Specifically, we find that the characteristic size δ (see Fig 14-right) associated with the potential gradient in this region is comparable to the Debye length. The latter also is larger than the minimum mesh size. It is therefore also possible that the effects of the sheath modify the structure of the potential in this region and, in turn, the ion divergence angle. This was also recognized early in the derivation of the magnetic shielding first principles and is currently under closer investigation.

IV. Conclusions

During a recent 2-yr proof-of-principle effort to demonstrate the first principles of magnetic shielding in Hall thrusters, it was shown by numerical simulations, plasma diagnostics and short wear tests of the H6 laboratory thruster that the erosion rates of the acceleration channel were reduced by 2-3 orders of magnitude compared to those in the unshielded version of the thruster. During the short wear tests roughening of most of the inner pole and part of the outer pole surfaces was also observed suggesting some sputtering could have occurred. In this paper we presented numerical simulations with the Hall2De code that aimed at quantifying the erosion rates of the inner pole where most of the surface roughening was detected. The simulations employed a new multi-fluid algorithm for the ion hydrodynamics to capture the low-energy ion populations that largely dominate the regions near the thruster poles. The simulations have shown that at a location near the outer radius of the inner pole the erosion rate exceeded the measured back-sputter rates thereby explaining in part the observed texture of the surface at that location. However, throughout the remainder of the inner pole the erosion rates were found to be below the back-sputter rates. It has been argued that the true position of the inner pole in the experiment could have allowed high-energy ions towards the pole surface due to the near-normal angle of the magnetic field lines with the exposed pole surface there. If true, then a simple mitigation technique was proposed involving thin graphite coating of the poles which is predicted to reduced erosion rates to at least 40 times below the back-sputter rate. At these rates the coating is expected to last thousands of kilohours. It has also been argued that the simulations could not capture fully the observed sputtering because the poles were modeled to be at the axial location as the exit plane. Under this geometry, most high-energy ions were found to be ejected away from the pole surface by the high electric field established immediately downstream of the exit plane, along the pole boundary.

Though plausible, it has also been recognized that the abovementioned mechanism for the surface roughening of the poles has been proposed based on a hydrodynamic simulation of ions. Because the ionized gas in the regions near the corners of the chamfered channel at the exit falls to very low densities, the sheath can grow to sizes that are sufficiently large to challenge the continuum assumption there. Therefore, the local physics in this region warrant special attention and is a topic of ongoing investigation. Moreover, though the first assessment we have performed under non-vacuum conditions suggested that the effects of the background neutrals on the computed erosion rates were not significant, more detailed simulations must be carried out that take into account the depletion of neutrals around the outer boundaries. These simulations must be supported by detailed measurements near the H6MS poles, to validate our predictions of plasma conditions in this region.

Acknowledgments

The research described in this paper was carried out by the Jet Propulsion Laboratory, California Institute of Technology, under a contract with the National Aeronautics and Space Administration.

References

[1] I. G. Mikellides, I. Katz, R. R. Hofer *et al.*, "Magnetic shielding of walls from the unmagnetized ion beam in a Hall thruster," *Applied Physics Letters*, vol. 102, no. 2, Jan 14, 2013.

[2] I. G. Mikellides, I. Katz, R. R. Hofer *et al.*, "Magnetic shielding of a laboratory Hall thruster. I. Theory and validation," *Journal of Applied Physics*, vol. 115, no. 4, Jan 28, 2014.

[3] R. R. Hofer, D. M. Goebel, I. G. Mikellides *et al.*, "Magnetic shielding of a laboratory Hall thruster. II. Experiments," *Journal of Applied Physics*, vol. 115, no. 4, Jan 28, 2014.

[4] I. G. Mikellides, and I. Katz, "Numerical simulations of Hall-effect plasma accelerators on a magnetic-field-aligned mesh," *Physical Review E*, vol. 86, no. 4, pp. 046703, Oct 17, 2012.

[5] I. G. Mikellides, I. Katz, R. R. Hofer *et al.*, "Magnetic shielding of the channel walls in a Hall plasma accelerator," *Physics of Plasmas*, vol. 18, no. 3, pp. 033501, Mar, 2011.

[6] K. H. De Grys, A. Mathers, B. Welander *et al.*, "AIAA Paper No. 10-6698," in Proceedings of the 46th AIAA/ASME/SAE/ASEE Joint Propulsion Conference, Nashville, TN, 2010, pp. 6698.

[7] J. M. Haas, R. R. Hofer, D. L. Brown *et al.*, in 54th JANNAF Propulsion Meeting, Denver, CO, 2007.

[8] I. G. Mikellides, R. R. Hofer, I. Katz *et al.*, "AIAA Paper No. 13-3885," in Proceedings of the 49th AIAA Joint Propulsion Conference, San Jose, CA, 2013, pp. 3885.

[9] R. R. Hofer, B. A. Jorns, J. E. Polk *et al.*, "IEPC Paper No. 13-033," in Proceedings of the 33rd International Electric Propulsion Conference, Washington, DC, 2013, pp. 033.

[10] J. R. Brophy, and L. Friedman, "Returning an Entire Near-Earth Asteroid in Support of Human Exploration Beyond Low-Earth Orbit," in IAF Global Exploration Conference, Washington, D. C., 2012.

[11] J. R. Brophy, L. Friedman, and F. Culick, "Asteroid Retrieval Feasibility," in Aerospace Conference, 2012, Big Sky, MT, 2012, pp. 1 - 16.

[12] J. R. Brophy, and S. Oleson, "AIAA Paper No. 12-4067," in Proceedings of the 48th AIAA Joint Propulsion Conference, Atlanta, GA, 2012, pp. 4067.

[13] H. Kamhawi, T. W. Haag, D. T. Jacobson *et al.*, "AIAA Paper No. 11-5521," in Proceedings of the 47th AIAA Joint Propulsion Conference, San Diego, CA, 2011, pp. 5809.

[14] R. R. Hofer, D. M. Goebel, I. G. Mikellides *et al.*, "AIAA Paper No. 12-3788," in Proceedings of the 48th AIAA Joint Propulsion Conference, Atlanta, GA, 2012, pp. 3788.

[15] I. G. Mikellides, I. Katz, R. R. Hofer *et al.*, "AIAA Paper No. 12-3789," in Proceedings of the 48th AIAA Joint Propulsion Conference, Atlanta, GA, 2012, pp. 3789.

[16] I. G. Mikellides, I. Katz, and R. R. Hofer, "AIAA Paper No. 11-5809," in Proceedings of the 47th AIAA Joint Propulsion Conference, San Diego, CA, 2011, pp. 5809.

[17] A. I. Morozov, "Focussing of Cold Quasineutral Beams in Electromagnetic Fields," *Doklady Akademii Nauk Sssr*, vol. 163, no. 6, pp. 1363-&, 1965.

[18] A. I. Morozov, and V. V. Savelyev, "Fundamentals of Stationary Plasma Thruster Theory Reviews of Plasma Physics," Reviews of Plasma Physics B. B. Kadomtsev and V. D. Shafranov, eds., pp. 203-391: Springer US, 2000.

[19] I. Katz, and I. G. Mikellides, "Neutral gas free molecular flow algorithm including ionization and walls for use in plasma simulations," *Journal of Computational Physics*, vol. 230, no. 4, pp. 1454-1464, Feb 20, 2011.

[20] A. L. Ortega, and I. G. Mikellides, "AIAA Paper No. 14-XXXX," in Proceedings of the 50th AIAA Joint Propulsion Conference, Cleveland, OH, 2014, pp. XXXX.

[21] N. B. Meezan, W. A. Hargus, and M. A. Cappelli, "Anomalous electron mobility in a coaxial Hall discharge plasma," *Physical Review E*, vol. 63, no. 2, pp. 026410, Feb, 2001.

[22] A. Ducrocq, J. C. Adam, A. Heron *et al.*, "High-frequency electron drift instability in the cross-field configuration of Hall thrusters," *Physics of Plasmas*, vol. 13, no. 10, Oct, 2006.

[23] A. Lazurenko, T. D. de Wit, C. Cavoit *et al.*, "Determination of the electron anomalous mobility through measurements of turbulent magnetic field in Hall thrusters," *Physics of Plasmas,* vol. 14, no. 3, Mar, 2007.
[24] C. Boniface, L. Garrigues, G. J. M. Hagelaar *et al.*, "Anomalous cross field electron transport in a Hall effect thruster," *Applied Physics Letters,* vol. 89, no. 16, Oct 16, 2006.
[25] J. C. Adam, A. Heron, and G. Laval, "Study of stationary plasma thrusters using two-dimensional fully kinetic simulations," *Physics of Plasmas,* vol. 11, no. 1, pp. 295-305, Jan, 2004.
[26] P. Coche, and L. Garrigues, "A two-dimensional (azimuthal-axial) particle-in-cell model of a Hall thruster," *Physics of Plasmas,* vol. 21, no. 2, Feb, 2014.
[27] G. D. Hobbs, and J. A. Wesson, "Heat Flow through a Langmuir Sheath in Presence of Electron Emission," *Plasma Physics,* vol. 9, no. 1, pp. 85-87, 1967.
[28] A. Harten, P. D. Lax, and B. Vanleer, "On Upstream Differencing and Godunov-Type Schemes for Hyperbolic Conservation-Laws," *Siam Review,* vol. 25, no. 1, pp. 35-61, 1983.
[29] J. C. Butcher, "Numerical methods for ordinary differential equations in the 20th century," *Journal of Computational and Applied Mathematics,* vol. 125, no. 1-2, pp. 1-29, Dec 15, 2000.
[30] I. G. Mikellides, I. Katz, R. R. Hofer *et al.*, "AIAA Paper No. 10-6942," in Proceedings of the 46th AIAA Joint Propulsion Conference, Nashville, TN, 2010, pp. 6942.
[31] J. M. Fife, "Hybrid-PIC modeling and electrostatic probe survey of Hall thrusters," Ph D, Massachusetts Institute of Technology, 1998.
[32] J. M. Fife, M. Martinez-Sanchez, and J. Szabo, "AIAA Paper No. 97-3052," in 33rd AIAA/ASMA/SAE/ASEE Joint Propulsion Conference, Seattle, WA, 1997, pp. 3052.
[33] M. K. Scharfe, N. Gascon, M. A. Cappelli *et al.*, "Comparison of hybrid Hall thruster model to experimental measurements," *Physics of Plasmas,* vol. 13, no. 8, Aug, 2006.
[34] E. Sommier, M. K. Scharfe, N. Gascon *et al.*, "Simulating Plasma-Induced Hall Thruster Wall Erosion With a Two-Dimensional Hybrid Model," *Plasma Science, IEEE Transactions on,* vol. 35, no. 5, pp. 1379-1387, 2007.
[35] w. A. Hargus, and M. A. Cappelli, "Investigation of the plasma acceleration mechanism within a coaxial Hall thruster," Thesis (Ph D), Stanford University, 2001., 2001.
[36] C. A. Thomas, and M. A. Cappelli, "Anomalous electron transport in the Hall-effect thruster," Thesis (Ph D), Stanford University, 2007., 2006.
[37] B. A. Jorns, R. R. Hofer, and D. M. Goebel, "Study of Probe Perturbation Effects in the H6US," Jet Propulsion Laboratory, California Institute of Technology, 2014, p. 52.
[38] K. K. Jameson, "Investigation of hollow cathode effects on total thruster efficiency in a 6 kW Hall thruster," Ph D, UCLA, 2008.
[39] A. L. Ortega, I. Katz, I. G. Mikellides *et al.*, "Self-consistent Model of a High Power Hall Thruster Plume," in 13th Spacecraft Charging Technologies Conference, Pasadena, CA, June 23-27, 2014, 2014.
[40] R. R. Hofer, I. G. Mikellides, I. Katz *et al.*, "AIAA Paper No. 07-5267," in Proceedings of the 43rd AIAA Joint Propulsion Conference, Cincinnati, OH, 2007, pp. 5267.
[41] D. Rosenberg, and G. K. Wehner, "Sputtering Yields for Low Energy He+-, Kr+-, and Xe+-Ion Bombardment," *Journal of Applied Physics,* vol. 33, no. 5, pp. 1842-&, 1962.
[42] R. P. Doerner, D. G. Whyte, and D. M. Goebel, "Sputtering yield measurements during low energy xenon plasma bombardment," *Journal of Applied Physics,* vol. 93, no. 9, pp. 5816-5823, May 1, 2003.
[43] J. Bohdansky, "A Universal Relation for the Sputtering Yield of Monatomic Solids at Normal Ion Incidence," *Nuclear Instruments & Methods in Physics Research Section B-Beam Interactions with Materials and Atoms,* vol. 2, no. 1-3, pp. 587-591, 1984.